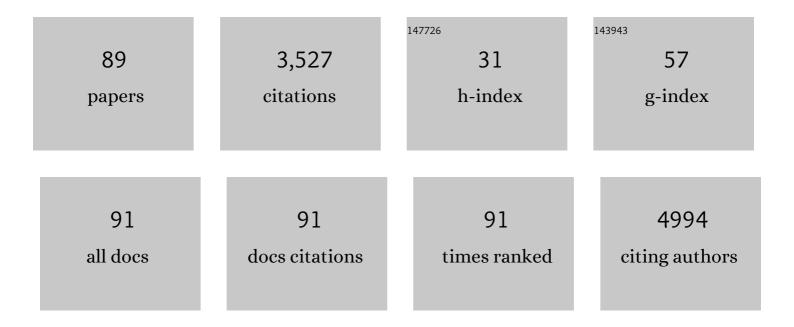
List of Publications by Year in descending order

Source: https://exaly.com/author-pdf/5488368/publications.pdf Version: 2024-02-01



IENS NIVIAS

#	Article	IF	CITATIONS
1	Millisecond Coherence Time in a Tunable Molecular Electronic Spin Qubit. ACS Central Science, 2015, 1, 488-492.	5.3	296
2	Sodium insertion in carboxylate based materials and their application in 3.6 V full sodium cells. Energy and Environmental Science, 2012, 5, 9632.	15.6	235
3	Ultrafast Transient Absorption Studies on Photosystem I Reaction Centers from Chlamydomonas reinhardtii. 1. A New Interpretation of the Energy Trapping and Early Electron Transfer Steps in Photosystem I. Biophysical Journal, 2003, 85, 3899-3922.	0.2	180
4	Selective propane dehydrogenation with single-site Coll on SiO2 by a non-redox mechanism. Journal of Catalysis, 2015, 322, 24-37.	3.1	168
5	Ultrafast Transient Absorption Studies on Photosystem I Reaction Centers from Chlamydomonas reinhardtii. 2: Mutations near the P700 Reaction Center Chlorophylls Provide New Insight into the Nature of the Primary Electron Donor. Biophysical Journal, 2006, 90, 552-565.	0.2	146
6	Highly-efficient charge separation and polaron delocalization in polymer–fullerene bulk-heterojunctions: a comparative multi-frequency EPR and DFT study. Physical Chemistry Chemical Physics, 2013, 15, 9562.	1.3	135
7	Long Coherence Times in Nuclear Spin-Free Vanadyl Qubits. Journal of the American Chemical Society, 2016, 138, 14678-14685.	6.6	118
8	Manganese in Graphite Anode and Capacity Fade in Li Ion Batteries. Journal of Physical Chemistry C, 2014, 118, 24335-24348.	1.5	115
9	Nitrogen-Defective Polymeric Carbon Nitride Nanolayer Enabled Efficient Electrocatalytic Nitrogen Reduction with High Faradaic Efficiency. Nano Letters, 2020, 20, 2879-2885.	4.5	92
10	Hydrogen Bonding to P700:  Site-Directed Mutagenesis of Threonine A739 of Photosystem I in Chlamydomonas reinhardtii,. Biochemistry, 2002, 41, 8557-8569.	1.2	88
11	Protein Delivery of a Ni Catalyst to Photosystem I for Light-Driven Hydrogen Production. Journal of the American Chemical Society, 2013, 135, 13246-13249.	6.6	83
12	Optical charge state control of spin defects in 4H-SiC. Nature Communications, 2017, 8, 1876.	5.8	83
13	Multiple Quantum Coherences from Hyperfine Transitions in a Vanadium(IV) Complex. Journal of the American Chemical Society, 2014, 136, 15841-15844.	6.6	81
14	Cobaloxime-Based Artificial Hydrogenases. Inorganic Chemistry, 2014, 53, 8071-8082.	1.9	78
15	Charge Transfer Processes in OPV Materials as Revealed by EPR Spectroscopy. Advanced Energy Materials, 2017, 7, 1602226.	10.2	75
16	Photo-accelerated fast charging of lithium-ion batteries. Nature Communications, 2019, 10, 4946.	5.8	68
17	Charge Recombination Fluorescence in Photosystem I Reaction Centers fromChlamydomonas reinhardtii. Journal of Physical Chemistry B, 2005, 109, 5903-5911.	1.2	66
18	Ligand Transformations and Efficient Proton/Water Reduction with Cobalt Catalysts Based on Pentadentate Pyridineâ€Rich Environments. Angewandte Chemie - International Edition, 2015, 54, 2105-2110.	7.2	61

#	Article	IF	CITATIONS
19	Through-Space Ultrafast Photoinduced Electron Transfer Dynamics of a C ₇₀ -Encapsulated Bisporphyrin Covalent Organic Polyhedron in a Low-Dielectric Medium. Journal of the American Chemical Society, 2017, 139, 4286-4289.	6.6	58
20	Discovery of Highly Selective Alkyne Semihydrogenation Catalysts Based on Firstâ€Row Transitionâ€Metallated Porous Organic Polymers. Angewandte Chemie - International Edition, 2014, 53, 12055-12058.	7.2	51
21	Supported Single-Site Ti(IV) on a Metal–Organic Framework for the Hydroboration of Carbonyl Compounds. Organometallics, 2017, 36, 3921-3930.	1.1	50
22	The Hydrogen Catalyst Cobaloxime: A Multifrequency EPR and DFT Study of Cobaloxime's Electronic Structure. Journal of Physical Chemistry B, 2012, 116, 2943-2957.	1.2	48
23	Photoinduced Dynamics of Charge Separation: From Photosynthesis to Polymer–Fullerene Bulk Heterojunctions. Journal of Physical Chemistry B, 2015, 119, 7407-7416.	1.2	48
24	Aqueous light driven hydrogen production by a Ru–ferredoxin–Co biohybrid. Chemical Communications, 2015, 51, 10628-10631.	2.2	45
25	Semi-artificial Photosynthetic CO ₂ Reduction through Purple Membrane Re-engineering with Semiconductor. Journal of the American Chemical Society, 2019, 141, 11811-11815.	6.6	44
26	Molecular Cobalt Catalysts for H ₂ Generation with Redox Activity and Proton Relays in the Second Coordination Sphere. Inorganic Chemistry, 2019, 58, 1697-1709.	1.9	44
27	Zirconium Modification Promotes Catalytic Activity of a Single-Site Cobalt Heterogeneous Catalyst for Propane Dehydrogenation. ACS Omega, 2018, 3, 11117-11127.	1.6	43
28	Electronic Structure of the Quinone Radical Anion A ₁ ^{•â^'} of Photosystem I Investigated by Advanced Pulse EPR and ENDOR Techniques. Journal of Physical Chemistry B, 2009, 113, 10367-10379.	1.2	42
29	Complex Relationship between Side-Chain Polarity, Conductivity, and Thermal Stability in Molecularly Doped Conjugated Polymers. Chemistry of Materials, 2021, 33, 741-753.	3.2	36
30	Evaluation of the coordination preferences and catalytic pathways of heteroaxial cobalt oximes towards hydrogen generation. Chemical Science, 2016, 7, 3264-3278.	3.7	35
31	Phylloquinone and Related Radical Anions Studied by Pulse Electron Nuclear Double Resonance Spectroscopy at 34 GHz and Density Functional Theory. Journal of Physical Chemistry B, 2006, 110, 11549-11560.	1.2	34
32	Ru–protein–Co biohybrids designed for solar hydrogen production: understanding electron transfer pathways related to photocatalytic function. Chemical Science, 2016, 7, 7068-7078.	3.7	32
33	Spin-Density Distribution of the Carotenoid Triplet State in the Peridinin-Chlorophyll-Protein Antenna. A Q-Band Pulse Electron-Nuclear Double Resonance and Density Functional Theory Study. Journal of the American Chemical Society, 2007, 129, 15442-15443.	6.6	31
34	Electronic Structure of Fullerene Heterodimer in Bulkâ€Heterojunction Blends. Advanced Energy Materials, 2014, 4, 1301517.	10.2	30
35	Structure Control of a π-Conjugated Oligothiophene-Based Liquid Crystal for Enhanced Mixed Ion/Electron Transport Characteristics. ACS Nano, 2019, 13, 7665-7675.	7.3	29
36	Detection of a charge-separated catalyst precursor state in a linked photosensitizer-catalyst assembly. Physical Chemistry Chemical Physics, 2013, 15, 21070.	1.3	28

#	Article	IF	CITATIONS
37	Orientation Resolving Dipolar High-Field EPR Spectroscopy on Disordered Solids: II. Structure of Spin-Correlated Radical Pairs in Photosystem I. Journal of Physical Chemistry B, 2013, 117, 11184-11199.	1.2	27
38	Synthesis and Catalytic Hydrogenation Reactivity of a Chromium Catecholate Porous Organic Polymer. Organometallics, 2015, 34, 947-952.	1.1	27
39	Isolated, well-defined organovanadium(<scp>iii</scp>) on silica: single-site catalyst for hydrogenation of alkenes and alkynes. Chemical Communications, 2017, 53, 7325-7328.	2.2	26
40	Artificial Hydrogenases Based on Cobaloximes and Heme Oxygenase. ChemPlusChem, 2016, 81, 1083-1089.	1.3	25
41	Mononuclear nickel (II) and copper (II) coordination complexes supported by bispicen ligand derivatives: Experimental and computational studies. Inorganica Chimica Acta, 2017, 455, 221-230.	1.2	25
42	In the Bottlebrush Garden: The Structural Aspects of Coordination Polymer Phases formed in Lanthanide Extraction with Alkyl Phosphoric Acids. Journal of Physical Chemistry B, 2015, 119, 11910-11927.	1.2	24
43	Triplet–triplet energy transfer in artificial and natural photosynthetic antennas. Proceedings of the National Academy of Sciences of the United States of America, 2017, 114, E5513-E5521.	3.3	24
44	Charge Separation Related to Photocatalytic H ₂ Production from a Ru–Apoflavodoxin–Ni Biohybrid. ACS Energy Letters, 2017, 2, 230-237.	8.8	20
45	Z-scheme solar water splitting <i>via</i> self-assembly of photosystem I-catalyst hybrids in thylakoid membranes. Chemical Science, 2018, 9, 8504-8512.	3.7	20
46	Intramolecular Hydrogen Bonding Restricts Gd–Aquaâ€Ligand Dynamics. Angewandte Chemie - International Edition, 2017, 56, 5603-5606.	7.2	19
47	Charge Separation and Triplet Exciton Formation Pathways in Small-Molecule Solar Cells as Studied by Time-Resolved EPR Spectroscopy. Journal of Physical Chemistry C, 2017, 121, 22707-22719.	1.5	19
48	Immobilization of an Amphiphilic Molecular Cobalt Catalyst on Carbon Black for Ligand-Assisted Water Oxidation. Inorganic Chemistry, 2018, 57, 9748-9756.	1.9	18
49	Incorporation of 2,3-Disubstituted-1,4-Naphthoquinones into the A1 Binding Site of Photosystem I Studied by EPR and ENDOR Spectroscopy. Applied Magnetic Resonance, 2010, 37, 65-83.	0.6	17
50	Mechanistic Aspects of a Surface Organovanadium(III) Catalyst for Hydrocarbon Hydrogenation and Dehydrogenation. ACS Catalysis, 2019, 9, 11055-11066.	5.5	17
51	<i>sp</i> ³ -Functionalization of Single-Walled Carbon Nanotubes Creates Localized Spins. ACS Nano, 2020, 14, 17675-17682.	7.3	17
52	Photoregeneration of Biomimetic Nicotinamide Adenine Dinucleotide Analogues via a Dye-Sensitized Approach. ACS Applied Energy Materials, 2019, 2, 80-91.	2.5	15
53	Electronic Structure of Fullerene Acceptors in Organic Bulk-Heterojunctions: A Combined EPR and DFT Study. Journal of Physical Chemistry Letters, 2015, 6, 4730-4735.	2.1	14
54	Absolute signs of hyperfine coupling constants as determined by pulse ENDOR of polarized radical pairs. Applied Magnetic Resonance, 2006, 30, 311-327.	0.6	13

#	Article	IF	CITATIONS
55	EPR, ENDOR, and Special TRIPLE measurements of P•+ in wild type and modified reaction centers from Rb.Asphaeroides. Photosynthesis Research, 2009, 99, 1-10.	1.6	13
56	Charge Separation in P3HT:SWCNT Blends Studied by EPR: Spin Signature of the Photoinduced Charged State in SWCNT. Journal of Physical Chemistry Letters, 2014, 5, 601-606.	2.1	13
57	X-ray Crystallographic, Multifrequency Electron Paramagnetic Resonance, and Density Functional Theory Characterization of the Ni(P ^{Cy} ₂ N ^{<i>t</i>Bu} ₂) ₂ ^{<i>n</i>Hydrogen Oxidation Catalyst in the Ni(I) Oxidation State. Inorganic Chemistry. 2015. 54. 6226-6234.}	1.9	13
58	Effects of denticity and ligand rigidity on reactivity of copper complexes with cumyl hydroperoxide. Inorganica Chimica Acta, 2018, 483, 71-78.	1.2	13
59	Surface immobilized copper(<scp>i</scp>) diimine photosensitizers as molecular probes for elucidating the effects of confinement at interfaces for solar energy conversion. Chemical Communications, 2020, 56, 12130-12133.	2.2	13
60	Light induced electron spin resonance properties of van der Waals CrX3 (X = Cl, I) crystals. Applied Physics Letters, 2020, 117, .	1.5	12
61	Correlating conductivity and Seebeck coefficient to doping within crystalline and amorphous domains in poly(3â€{methoxyethoxyethoxy)thiophene). Journal of Polymer Science, 2021, 59, 2797-2808.	2.0	11
62	An Active‧ite Sulfonate Group Creates a Fast Water Oxidation Electrocatalyst That Exhibits High Activity in Acid. Angewandte Chemie - International Edition, 2021, 60, 1540-1545.	7.2	10
63	FTIR spectroscopy shows structural similarities between photosystems II from cyanobacteria and spinach. FEBS Journal, 2004, 271, 563-567.	0.2	9
64	Pulse Q-Band EPR and ENDOR Spectroscopies of the Photochemically Generated Monoprotonated Benzosemiquinone Radical in Frozen Alcoholic Solution. Journal of Physical Chemistry B, 2012, 116, 8890-8900.	1.2	9
65	Nuclearity effects in supported, single-site Fe(<scp>ii</scp>) hydrogenation pre-catalysts. Dalton Transactions, 2018, 47, 10842-10846.	1.6	9
66	Primary donor triplet states of Photosystem I and II studied by Q-band pulse ENDOR spectroscopy. Photosynthesis Research, 2022, , 1.	1.6	9
67	Spin Signature of the C ₆₀ Fullerene Anion: A Combined X- and D-Band EPR and DFT Study. Journal of Physical Chemistry Letters, 2018, 9, 3915-3921.	2.1	8
68	Spin-Correlated Radical Pairs as Quantum Sensors of Bidirectional ET Mechanisms in Photosystem I. Journal of Physical Chemistry B, 2019, 123, 7536-7544.	1.2	8
69	Insights into the extraction of photogenerated holes from CdSe/CdS nanorods for oxidative organic catalysis. Journal of Materials Chemistry A, 2021, 9, 12690-12699.	5.2	8
70	Investigation of the Stationary and Transient A 1 ·â^' Radical in TrpÂ→ÂPhe Mutants of Photosystem I. Applied Magnetic Resonance, 2010, 38, 187-203.	0.6	7
71	Electron Paramagnetic Resonance Characterization of the Triheme Cytochrome from <i>Geobacter sulfurreducens</i> . Biochemistry, 2018, 57, 1722-1732.	1.2	6
72	Observation of current rectification by the new bimetallic iron(<scp>iii</scp>) hydrophobe [FeIII2(L ^{N4O6})] on Au LB-molecule Au devices. Dalton Transactions, 2018, 47, 14352-14361.	1.6	6

#	Article	IF	CITATIONS
73	Lithium-Ion Battery Materials as Tunable, "Redox Non-Innocent―Catalyst Supports. ACS Catalysis, 0, , 7233-7242.	5.5	6
74	Polaron and Exciton Delocalization in Oligomers of High-Performance Polymer PTB7. Journal of the American Chemical Society, 2020, 142, 1359-1366.	6.6	5
75	Structural and Functional Characterization of a Short-Chain Flavodoxin Associated with a Noncanonical 1,2-Propanediol Utilization Bacterial Microcompartment. Biochemistry, 2017, 56, 5679-5690.	1.2	4
76	Reactivity of bio-inspired Cu(II) (N2/Py2) complexes with peroxide at room temperature. Journal of Inorganic Biochemistry, 2019, 197, 110674.	1.5	4
77	Interprotein electron transfer biohybrid system for photocatalytic H2 production. Photosynthesis Research, 2020, 143, 183-192.	1.6	4
78	An Active‣ite Sulfonate Group Creates a Fast Water Oxidation Electrocatalyst That Exhibits High Activity in Acid. Angewandte Chemie, 2021, 133, 1564-1569.	1.6	4
79	Replacing Pyridine with Pyrazine in Molecular Cobalt Catalysts: Effects on Electrochemical Properties and Aqueous H2 Generation. Catalysts, 2021, 11, 75.	1.6	4
80	Structure–Transport Properties Governing the Interplay in Humidity-Dependent Mixed Ionic and Electronic Conduction of Conjugated Polyelectrolytes. ACS Polymers Au, 2022, 2, 275-286.	1.7	4
81	Changing the site energy of per-614 in the Peridinin-chlorophyll a-protein does not alter its capability of chlorophyll triplet quenching. Biochimica Et Biophysica Acta - Bioenergetics, 2018, 1859, 612-618.	0.5	3
82	Charge Transfer: Electronic Structure of Fullerene Heterodimer in Bulkâ€Heterojunction Blends (Adv.) Tj ETQq0 (0 o rgBT /0 10.2	Overlock 10 Tr
83	Intramolecular Hydrogen Bonding Restricts Gd–Aquaâ€Ligand Dynamics. Angewandte Chemie, 2017, 129, 5695-5698.	1.6	2
84	Biohybrid photosynthetic charge accumulation detected by flavin semiquinone formation in ferredoxin-NADP ⁺ reductase. Chemical Science, 2022, 13, 6502-6511.	3.7	2
85	Donor–Acceptor Conjugated Copolymers Containing Transition-Metal Complex: Intrachain Magnetic Exchange Interactions and Magneto-Optical Activity. Chemistry of Materials, 0, , .	3.2	2
86	One Electron Multiple Proton Transfer in Model Organic Donor–Acceptor Systems: Implications for High-Frequency EPR. Applied Magnetic Resonance, 2020, 51, 977-991.	0.6	1
87	Dâ€Band EPR and ENDOR Spectroscopy of 15N‣abeled Photosystem I. Applied Magnetic Resonance, 0, , 1.	0.6	1
88	Efficient Intrinsic Photoprotection in Strongly Coupled (Bacterio) Chloropyll Complexes. Biophysical Journal, 2012, 102, 167a.	0.2	0
89	Organic Photovoltaics: Charge Transfer Processes in OPV Materials as Revealed by EPR Spectroscopy (Adv. Energy Mater. 10/2017). Advanced Energy Materials, 2017, 7, .	10.2	Ο